Three-dimensional simulation and localization of power cable fault point by combining wavelet transform and neural network

Yuning-Tao*

- College of Electrical Engineering and New Energy, China Three Gorges University, Yichang, Hubei, 443000, China
- taoyuning12@163.com

Reception: 20 April 2024 | **Acceptance**: 6 May 2024 | **Publication**: 14 June 2024

Suggested citation:

Tao Yuning (2024). **Three-dimensional simulation and localization of power cable fault point by combining wavelet transform and neural network.** 3C Tecnología. Glosas de innovación aplicada a la pyme. 13 (1), 35-55. https://doi.org/10.17993/3ctecno.2024.v13n1e45.35-55

ABSTRACT

This study centers on the 3D simulation localization technology of power cable fault points, using the combination of wavelet transform and neural network, aiming to improve the accuracy and efficiency of cable fault localization. This paper adopts the method of combining wavelet transform and genetic algorithm optimization of back propagation (GA-BP) neural network. First, by constructing a three-dimensional simulation model of power cables, the wavelet transform is applied to extract fault features and the GA-BP neural network is utilized for fault point localization. The experimental results show that the average localization errors of this method in single-phase ground fault and two-phase grounded short-circuit fault are 0.112km and 0.126km, respectively, which are significantly better than the traditional method. Under different fault initial phase angle conditions, the proposed method shows strong adaptability and the error is controlled within 1%. Meanwhile, the present algorithm exhibits strong noise suppression ability under white and colored noise backgrounds, especially in low signal-to-noise ratio environments. In summary, this study demonstrates the effectiveness of the 3D simulation localization technique for power cable fault points combining wavelet transform and GA-BP neural network in improving the localization accuracy and noise resistance.

KEYWORDS

Power cable, three-dimensional simulation, wavelet transform, GA-BP neural network

https://doi.org/10.17993/3ctecno.2024.v13n1e45.35-55

INDEX

https://doi.org/10.17993/3ctecno.2024.v13n1e45.35-55

1. INTRODUCTION

China's urban power distribution network distribution form can be mainly divided into cable lines and overhead lines, the former has higher requirements for the installation environment and installation technology, but has the advantages of small power loss and strong stability, so power cables are widely used in undersea tunnels, transformer stations and other complex environments [1-3]. However, the installation environment of power cables determines the difficulty index of its fault detection increases linearly, compared with overhead lines, it is very difficult to diagnose and repair power cable faults in complex hidden environments such as undersea, underground, etc. [4-6].

With the rapid development of electric power science and technology, power cables have gradually become the "main artery" of power transmission in major cities. The overloaded operation of the power grid or long time use, will bring great burden to the power cable, and then appear low resistance failure, high resistance failure and other conditions. After the cable failure, rapid and accurate fault location, rapid restoration of reliable power supply, not only effectively reduce the fault outage time, but also reduce economic losses [7-8]. Due to the construction cost, cable channel conditions, power supply, accuracy and reliability and other factors, cable online monitoring and fault location technology has not yet been fully implemented, is still mainly offline testing for cable fault location [9-10].

Power cable fault diagnosis and localization techniques have been improved to reduce the outage time and maintenance cycle, as well as to enable fast power supply to the faulty local grid, to detect the operation of transmission lines and to reduce the economic losses.Li, G. et al. explored how to diagnose and locate the aging or deterioration of power cables by using impedance spectroscopy, and pointed out that the optimal frequency range of impedance spectrum analysis and a set of criteria for assessing the condition of cables can be determined by the reference frequency and the characteristic frequency, respectively. The reference frequency and characteristic frequency can be used to determine the optimal frequency range for impedance spectral analysis and a set of criteria for assessing the condition of cables, which is easier to diagnose and locate the aging of cables than previous methods, and the measurement process is simpler [11]. Li, M. et al. proposed a fault location method based on traveling waves, and improved it with an autonomous learning algorithm. Simulation experiments of the improved localization method on typical power cable circuits were carried out using PSCAD, and the results confirmed that the improved algorithm is fully capable of identifying short-circuit faults in power cable systems [12].Sommervogel, L. pointed out several types of faults that may be encountered during the detection of a cable's entire lifecycle and used a new methodology for modeling to conduct the study by combining measurement and simulation to improve the fault identification process [11]. measurement and simulation to improve the accuracy of fault localization, and the conclusions of the study provide an important reference for the practical application of cables [13].Tian, Y et al. conceptualized a method to conductive frequency protection of underground cables in closed-loop

https://doi.org/10.17993/3ctecno.2024.v13n1e45.35-55

distribution networks by using the current phase comparison method, which is executed through the remote unit (rtu) in the DAS, and the PSCAD simulation model is used, which verifies that the method can be used to locate and isolate the faults in time, and the application scenarios. locate and isolate faults with a wide range of application scenarios [14].Li, Z. et al. envisioned a deep-learning based cable infrared image state assessment method to measure the temperature of power cables, and based on the results of the statistical analysis, it was noted that this method can provide an effective and accurate state identification of the infrared maps of the cables [15].Siodla, K. et al. elaborated on the management of the medium-voltage cable network and the fault rate analysis of the current state of the art to manage MV cable networks by evaluating and diagnosing the operational status of individual cable lines obtained, these studies and conclusions are important references for cable line diagnostic studies [16].Samet, H. et al. conceptualized a method for the detection of early faults and differentiated such faults from other kinds of similar faults in the power system. The feasibility of the method was confirmed by simulation detection of four different arc models and analysis of actual fault data [17].Li, C. et al. investigated for the first time the effect of arc size on fire and flame propagation of 110 kV cross-linked polyethylene cables under the setting of constant power in arc discharge. After analog simulation testing, it was found that the larger the arc size, the more rapid the ignition rate of the cable fire, and the flame propagation in both vertical and horizontal azimuths increased significantly, which is of great significance for the prevention of and education about cable fires [18].A new distance-protection algorithm was proposed by Vinícius A. et al. to improve the protection of multi-terminal high-voltage direct current (MTDC) systems, and the feasibility of this algorithm was demonstrated by four-segment MTDC system detection and real-time simulation, which can provide more program choices for multi-terminal DC protection [19].

In this paper, the cable discharge data are collected and processed to build a model to simulate the actual fault scenario. Then, the wavelet transform technique is used to extract fault features, and the weights and thresholds of the backpropagation (BP) neural network are optimized by genetic algorithm (GA) to improve the training efficiency and accuracy of the network. Ultimately, the optimized GA-BP neural network is used to accurately locate the fault point. This process not only focuses on improving the accuracy of localization, but also considers the robustness of the algorithm in different noise environments.

2. THREE-DIMENSIONAL SIMULATION OF POWER CABLE FAULT POINT LOCALIZATION METHODS

2.1. CONSTRUCTING THREE-DIMENSIONAL SIMULATION MODELS OF POWER CABLES

The design of the three-dimensional simulation model of power cable needs to be based on data, that is, the collection of three-dimensional data, the establishment of

https://doi.org/10.17993/3ctecno.2024.v13n1e45.35-55

visualization information collection program, and the summary of the collected data to build a database. Power cable discharge data acquisition process, inevitably contains part of the noise information, resulting in poor authenticity of the three-dimensional model, to which this paper adopts the use of the Internet of Things and ZigBee networking real-time adjustment of the discharge signal data, to generate a three-dimensional visualization model of the power cable. After the partition block processing of the power cable, the fuzzy pixel value of the three-dimensional visual information acquisition is expressed as:

$$g(x,y) = h(x,y) * \eta(x,y) \tag{1}$$

Where (x,y) denotes the pixel value, *g* denotes the visual information sampling result, *h* denotes the set of association rules for 3D information sampling of power cables, * denotes the convolution, and η denotes the interference information.

Based on the above calculation results, fusing the collected data of each block, the template matching method is applied to establish a statistical analysis model that can be used for fault point localization. The vector of three-dimensional features of the power cable model is represented as:

$$t = A_s + ns \tag{2}$$

Where t denotes the 3D feature vector, n denotes the dimension of the 3D simulation model of power cables, s denotes the partition block, and A_s denotes the partition block vector fusion value. Figure 1 shows the three-dimensional simulation design architecture, according to which the purpose of human-computer interaction is achieved in the process of cable fault point localization. Using the results of the above vector value calculation, the three-dimensional simulation model of power cables is constructed in the embedded control platform. In order to strengthen the authenticity of the three-dimensional simulation model of power cables, it is necessary to enhance the efficiency of the screen rendering, and the comprehensive consideration of a variety of modeling software such as 3DStudio, Lightware3D, Multigen Creator and other modeling software is analyzed to analyze the rendering efficiency of the software modeling, and then the Multigen Creator software is selected to meet the three-dimensional simulation design requirements. After analyzing the rendering efficiency of the software modeling. The application of Multigen Creator software combined with the three-dimensional feature vectors of the power cable model, the output vector modeling results, to meet the virtual real-time and efficient requirements of virtual three-dimensional model building.

https://doi.org/10.17993/3ctecno.2024.v13n1e45.35-55

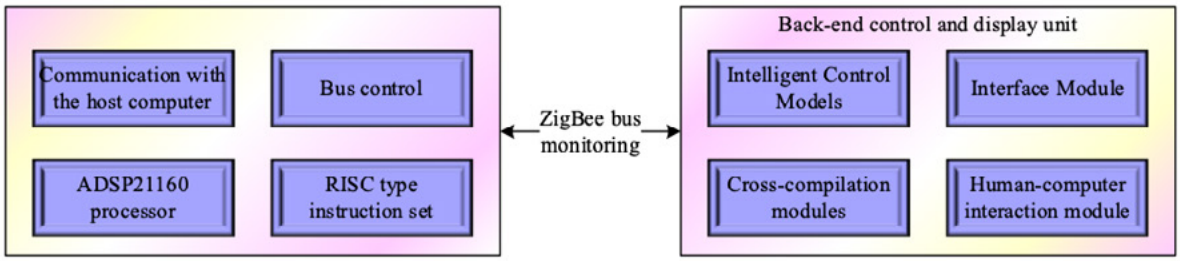

Figure 1 3D simulation design architecture

2.2. EXTRACTION OF THREE-DIMENSIONAL FEATURES OF POWER CABLES

Aiming at the three-dimensional simulation model of power cables, the analysis yields a three-dimensional feature distribution model for cable fault location:

$$\mu(n)=\begin{cases}\beta_1\left[1-\exp\left(-\alpha_1\left|e^n\right|^2\right)\right], & E_{[}\left|e^n\right|^2\geq K\\ \beta_2\left[1-\exp\left(-\alpha_2\left|e^n\right|^2\right)\right], & \text{Other}\end{cases} \tag{3}$$

Where K denotes the three-dimensional feature distribution information of power cable, μ denotes the three-dimensional feature distribution model, denotes the exponential function, e denotes the natural constant, E denotes the three-dimensional information reconstruction error, α_1 and $,\alpha_2,\beta_1$ β_2 ,denote the statistical eigenvalues. The specific constraints are:

$$\begin{cases}\alpha_1\geq 0,\alpha_2\geq 0\\ 0\leq\beta_1\leq\frac{1}{\lambda_{\max}},0\leq\beta_2\leq\frac{1}{\lambda_{\max}}\end{cases} \tag{4}$$

Where $\lambda_{\max}$ denotes the maximum feature screening amount. Combined with the principal component analysis algorithm, the database centered on 3D visual reconstruction data is constructed to ensure that the reconstruction results have a small error. The high-precision reconstruction of the 3D simulation model is completed by the above calculation results, and the feature information within the reconstructed model is collected using the information interaction mode, and the feature component output results are:

$$f=\sum_{i=1}^{n}\partial_i K+b \tag{5}$$

Where f denotes the feature component of the information interaction output, i denotes the spatial region, ∂_i denotes the modal value of the pixel point distribution

https://doi.org/10.17993/3ctecno.2024.v13n1e45.35-55

within the spatial *b* region, and denotes the dimensionality of the 3D visual reconstruction. The blurred center of mass of the view image is determined using 3D imaging technology, and the probability density function calculation formula for feature extraction is derived through 3D visual simulation:

$$\sigma(x,y \mid \mu_K) = \prod \theta_K \frac{1}{\sqrt{2}} \exp\left\{ -\frac{(x-\mu_K)^2}{2} \right\} \tag{6}$$

Where σ denotes the probability density function, μ denotes the skew angle of 3D feature extraction, and θ denotes the feature point edge roundness function. Using the continuous difference reconstruction algorithm, the power cable fault region is made to exhibit smoothness, and the three-dimensional smooth region is denoted as:

$$P = \sum \left(f_p\right) + \sum V_{p,q}\left(f_p, f_q\right) \tag{7}$$

Where *P* denotes the 3D smoothing region, *V* denotes the continuous difference function, and *(p,q)* denotes the coordinates of the fault localization region after 3D reconstruction of the power cable.

In order to ensure the accuracy of the three-dimensional feature extraction results, the image is divided into multiple sub-pixel blocks, and the feature extraction optimization formula is derived by superposition calculation:

$$f = \sum_{i=1}^{n} \left(\partial_i - \bar{\partial}_i\right) K + b \tag{8}$$

Formula, $\bar{\partial}_i$ denotes the modulus of the 3D eigenvolume at sub-pixel points.

2.3. CABLE FAULT POINT LOCALIZATION BASED ON WAVELET TRANSFORM AND GA-BP NEURAL NETWORK

The proposed wavelet transforms and GA-BP based power cable fault location model is shown in Fig. 2, which mainly contains wavelet transform and mode maxima search module, GA optimization module, BP neural training and prediction module.

https://doi.org/10.17993/3ctecno.2024.v13n1e45.35-55

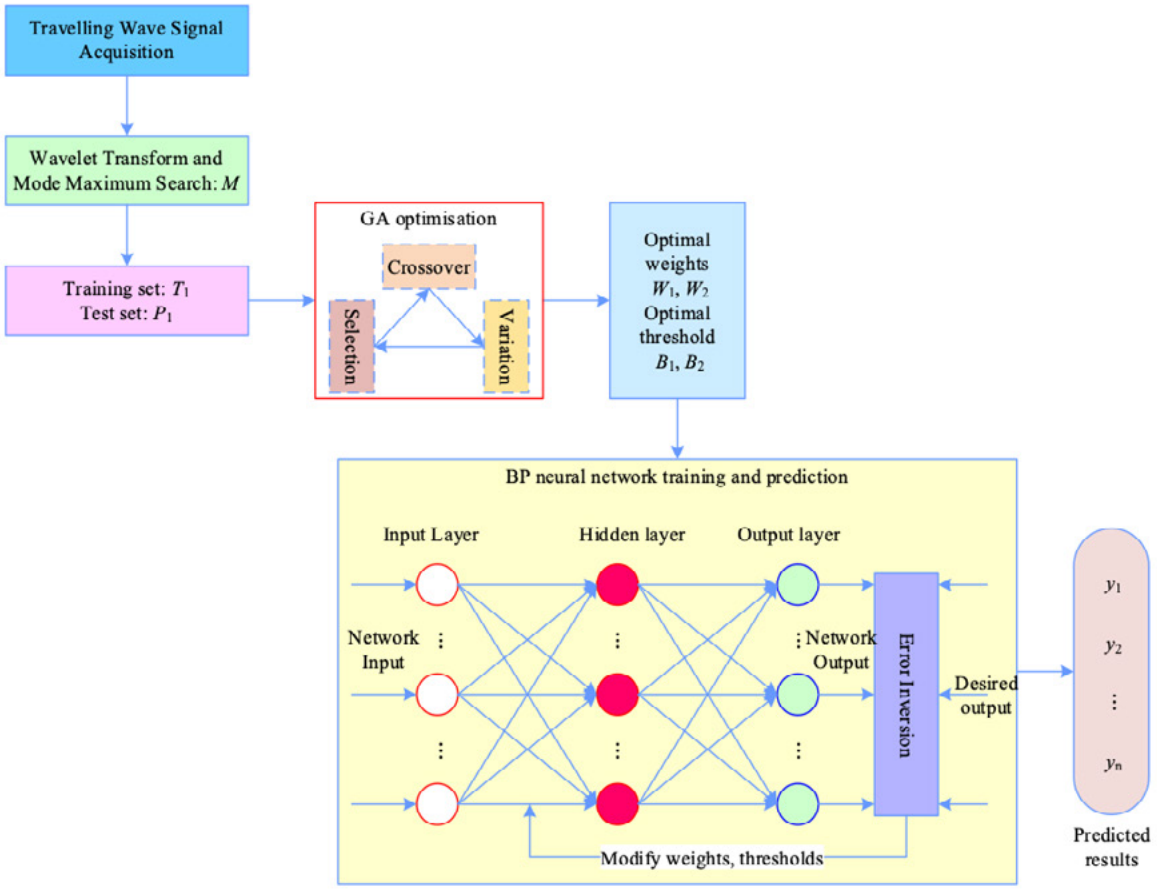

Figure 2 Fault location model of power cable based on wavelet transform and GA-BP

The flowchart of the wavelet transforms and GA-BP based power cable fault point localization algorithm is shown in Fig. 3, and the detailed steps are as follows.

The fault traveling wave mode maximum value data $M = \{(M_{11}, M_{12}), (M_{21}, M_{22}), \cdots (M_{n1}, M_{n2})\}$ collected on both sides of the cable is used as the feature value, and the set fault distance $X = \{X_1, X_2, \cdots X_3\}$ is used as the label value, which is normalized, and then the processed data is divided into the training data T_1 and the test data P_1, which are inputted into the GA-BP model.

Determine the topology of the BP neural network, the number of input layers inputnum, the number of hidden layers hiddennum and the number of output layers outputnum and initialize the BP neural network weights W1,W2 , threshold length B1, B2 .

GA optimizes the BP neural network module, determines the chromosome length and calculates the fitness by encoding the initial weight threshold of the BP neural network in real numbers, and constantly updates the fitness by selecting the function, crossover function and variation function.

https://doi.org/10.17993/3ctecno.2024.v13n1e45.35-55

Determine whether the end condition is satisfied, the number of termination iterations or a set threshold is reached. If it is not satisfied revert to the GA optimization step, if it is satisfied, the optimal weights and thresholds obtained are given to the BP neural network to complete the optimization purpose.

Retrain the BP neural network, calculate the error, and determine whether the end conditions are satisfied, if not, update the weights and thresholds. If the set error range is satisfied, simulation prediction is performed.

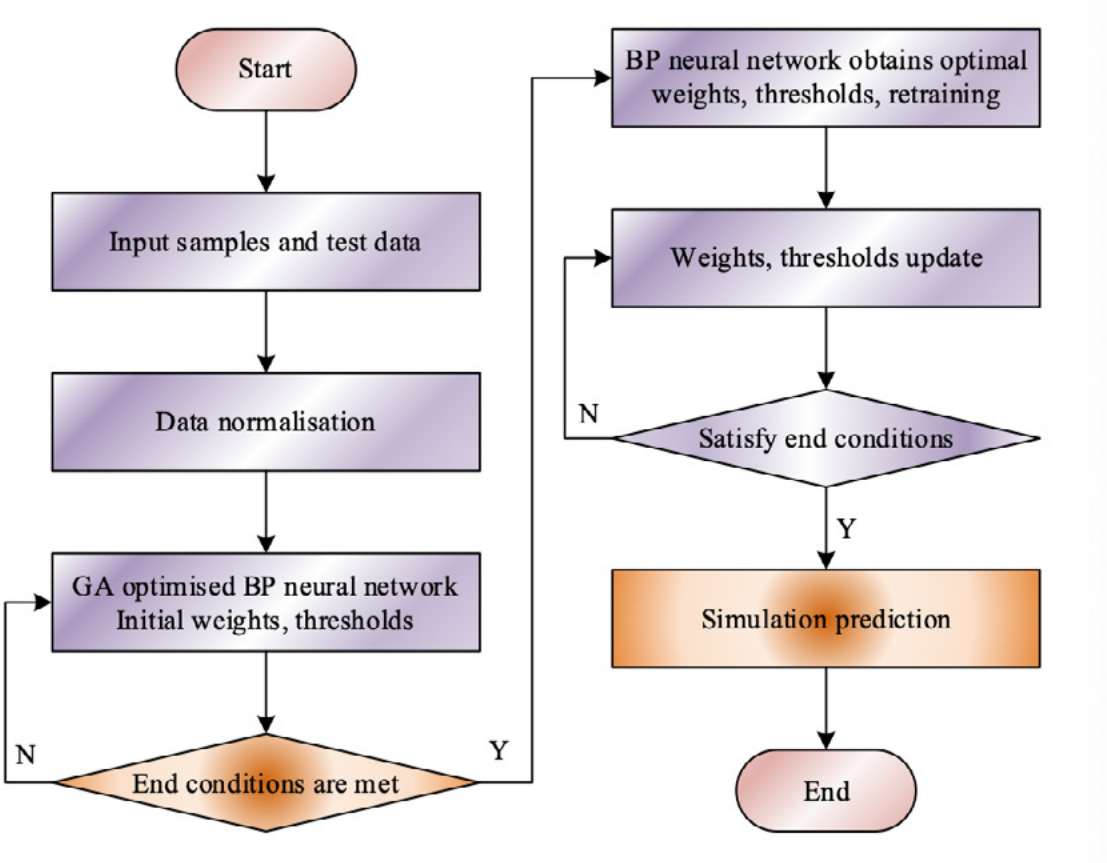

Figure 3 Power cable fault location flow chart

2.3.1. WAVELET TRANSFORM AND MODE MAXIMA SEARCH MODULE

When a power cable fault occurs, the transient traveling wave containing fault information will propagate in the cable, but because of its non-smooth and high frequency characteristics lead to the traveling wave head is difficult to identify, so the wavelet transform is used to analyze the good time-frequency domain characteristics and noise canceling ability to analyze the transient traveling wave, and the mode maxima theory is used to analyze the time of arrival of the initial head of faulty traveling wave.

(1) wavelet transform

https://doi.org/10.17993/3ctecno.2024.v13n1e45.35-55

Assuming that the Fourier transform $\psi(\omega)$ of $\psi(t)$ satisfies the admissibility condition, $\psi(t)$ can be called a mother wavelet:

$$C_\psi = \int_R \frac{|\psi(\omega)|^2}{\omega} d\omega < \infty \tag{9}$$

And for a continuous signal *g(t)* , its corresponding continuous wavelet transform (CWT) is:

$$CWT(a,b) = \frac{1}{\sqrt{a}} \int_R g(t) \overline{\psi\left(\frac{t-b}{a}\right)} dt \tag{10}$$

Where $\overline{\psi(t)}$ denotes the complex conjugate function of $\psi(t) \cdot a$ denotes the scale factor of the frequency-dependent wavelet function. *b* denotes the time-dependent displacement factor. However, in the process of practical application, it is necessary to discretize the continuous wavelet, assuming that $a = a_0^j$, $b = k a_0^j x b_0$, j, and $k \in Z$ can be obtained as the discrete wavelet transform (DWT):

$$DWT(j,k) = a_0^{-j/2} \psi\left(a_0^{-j} t - k b_0\right) \tag{11}$$

(2) Db6 Wavelet basis functions with mode maxima

Suppose there exists a simple step signal with the following functional expression:

$$S(t) = \begin{cases} 0 & 1 \le t \le 300 \\ 10 & 301 \le t \le 600 \end{cases} \tag{12}$$

This is an obvious signal with a mutation point, and according to the singularity principle, a singularity point is generated at the point.

The waveforms are more concentrated at the d1 scale and the moment of the step signal change can be clearly distinguished at 300s, so the modal maxima at the d1 scale will be collected as the characteristic vectors of the dataset. The method of determining the mode maxima is shown below.

Under a certain decomposition scale a_0, if there exists a point (a_0, b_0) such that $\frac{\partial\left(W_\psi f\right)(a_0,b_0)}{\partial b} = 0$, then ($a_0$, b_0) is called the local mode maxima. If $\left|\left(W_\psi f\right)(a_0,b)\right| \le \left|\left(W_\psi f\right)(a_0,b_0)\right|$ exists in any field of B0, then (a_0, b_0) is the mode maxima point of the wavelet transform coefficients. Therefore, in this paper, we use GA-BP neural network to train the mapping relationship between mode maxima

https://doi.org/10.17993/3ctecno.2024.v13n1e45.35-55

and fault location by taking the mode maxima data under the acquisition scale as the feature quantity and the distance to the fault is set as the label.

2.3.2. GA OPTIMIZATION MODULE

The use of traditional BP neural network for fault location in cables may cause the algorithm to fall into the local optimum or converge slowly because of the random initialization parameters of the network, in order to improve the convergence speed of the BP algorithm and the ability of global optimization searching, therefore, the introduction of GA to optimize the weights and thresholds of the BP neural network, the specific steps are as follows.

(1) Real number coding. The initial weights and thresholds of the BP neural network are encoded in real numbers with faster operation speed, utilizing the following linear transformation:

$$x(j) = p(j) + a(j)(q(j) - p(j)(j = 1, 2, \cdots, n) \qquad (13)$$

The initial change interval for the $[p(j), q(j)]$ interval of the *j* optimization variable *x(j)* corresponds to the $[0, 1]$ interval on the real number $a(j), a(j)$ in the genetic algorithm is expressed as genes, all the variables corresponding to the genes sequentially linked together to form a coded form of the solution to the problem $\left(a_1, a_2, \cdots a_k\right)$ is then called the individual or chromosome.

(2) Calculate the individual fitness. The initial weights and thresholds of the BP neural network are obtained according to the individual, and the output of the system is predicted after training the BP neural network with the training data, and the absolute value of the error between the predicted output and the desired output of the individual is taken as the value of the individual fitness *F*:

$$F = K\left(\sum_{i=1}^{n} abs\left(y_i - o_i\right)\right) \qquad (14)$$

n is the number of output nodes of the network. O_i is the desired output of the *i* th node of the *BP* neural network and y_i is the actual output of the *i* th node. *K* is the coefficient.

(3) Selection operation. Genetic algorithm selection operation betting roulette selection method, tournament selection method and geometric planning sorting selection and other methods, when selecting the roulette method, that is, based on the fitness ratio selection strategy, the selection probability P_i of each individual *i* is:

$$f_i = \frac{K}{F_i}, p_i = \frac{f_i}{\sum_{j=1}^{N} f_j} \qquad (15)$$

https://doi.org/10.17993/3ctecno.2024.v13n1e45.35-55

F_i is the fitness value of individual *i.* Since smaller fitness values are better, the inverse of fitness is taken before individual selection. *K* is the coefficient. *N* is the number of individuals in the population.

(4) Crossover operation. If the real number crossover method is used, the crossover operation of the *k* th chromosome a_k and the *l* th chromosome a_1 in the *j* dimension is as follows:

$$\begin{aligned} a_{kj} &= a_{kj}(1-b) + a_{lj}b \\ a_{lj} &= a_{lj}(1-b) + a_{kj}b \end{aligned} \tag{16}$$

Where *b* is a random number between .

(5) Mutation operation. The *j* th gene a_{ij} of the *i* th individual was selected for mutation:

$$a_{ij} = \begin{cases} a_{ij} + \left(a_{ij} - a_{\max}\right) * f(g) & r > 0.5 \\ a_{ij} + \left(a_{\min} - a_{ij}\right) * f(g) & r \le 0.5 \end{cases} \tag{17}$$

$$f(g) = r_2\left(1 - \frac{g}{G\max}\right)^2 \tag{18}$$

a_{max} is the upper bound of the gene a_{ij}. A_{min} is the lower bound of the gene. r_2 is a random number. *g* is the current iteration number. G_{max} is the maximum number of evolutions. *r* is a random number between $[0, 1]$.

(6) Calculate the individual fitness and determine whether the set end condition of minimum error is satisfied, if not, the operation of steps 3 to 5 is repeated. If the end condition is satisfied, the optimized weights and thresholds of the BP neural network are given.

2.3.3. BP NEURAL NETWORK TRAINING AND PREDICTION MODULE

The optimal weights and thresholds obtained through the GA optimization module are given to the BP neural network, and then the BP neural network is re-trained and predicted in the steps shown below.

(1) Select the transfer function and training function. Set the implicit layer transfer function, the output layer transfer function as and select the training function.

(2) Set other parameters of the BP neural network. The number of iterations epochs, learning rate learningrate, training target minimum error goal.

https://doi.org/10.17993/3ctecno.2024.v13n1e45.35-55

(3) Start training the BP neural network, and determine whether to meet the end conditions of setting the minimum error, if not, the weights and thresholds need to be re-updated. If satisfied, simulation prediction is carried out.

3. EXPERIMENTAL ANALYSIS OF FAULT POINT LOCALIZATION ALGORITHMS FOR POWER CABLES

3.1. SIMULATION ANALYSIS UNDER DIFFERENT FAULT INITIAL PHASE ANGLE CONDITIONS

This paper builds a power cable line with a total length of 70km, and the simulation model diagram of the power cable line is shown in Figure 4. Its voltage level is 110kV, 50Hz dual-source power supply system, single-phase ground fault occurs in phase A at 0.016s, the transition resistance is 100Ω, and the total simulation time is 0.05s. The total length of the hybrid line is 70km, of which the length of the overhead line is 50km and the length of the cable line is 20km.

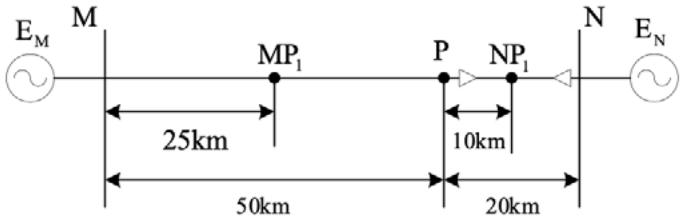

Figure 4 Schematic diagram of power cable line model

Faults may occur at any time in the power system, so the size of the initial phase angle of the fault has randomness. In order to verify that under different fault initial phase angle conditions, the power cable fault point localization algorithm in this paper has strong adaptability. In this subsection, different initial phase angles of faults at the same location are simulated and analyzed, and the values of initial phase angles of faults are set to be 0°, 30°, 45°, and the fault occurs at the 6km overhead line section as an example. Figure 5 shows the zero-mode component waveform curves of different faults, where (a)~(c) are the zero-mode component waveforms of the traveling wave of the faults on the M side of the bus, the cable junction point P and the N side of the bus, respectively. Although the zero-mode components at the same point may be slightly different for different initial phase angles of the fault, the general trend is the same, and the overall error does not exceed 5%. Therefore, for the case of short circuits with different initial phase angles of faults, the three-dimensional simulation and localization method based on wavelet transform and GA-BP power cable fault point proposed in this paper is still applicable to fault point localization.

https://doi.org/10.17993/3ctecno.2024.v13n1e45.35-55

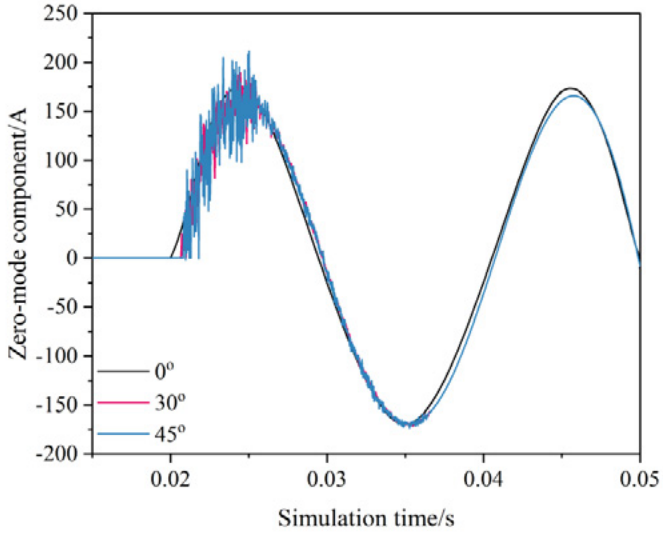

(a) Waveform diagram of zero mode component at point M

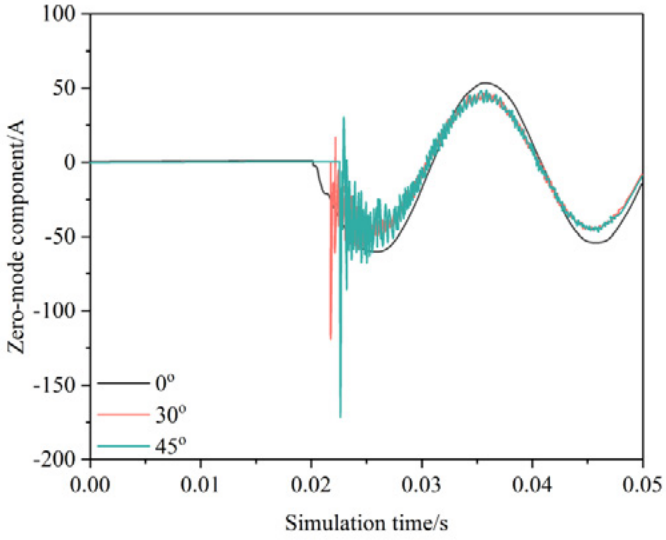

(b) Waveform diagram of zero mode component at point P

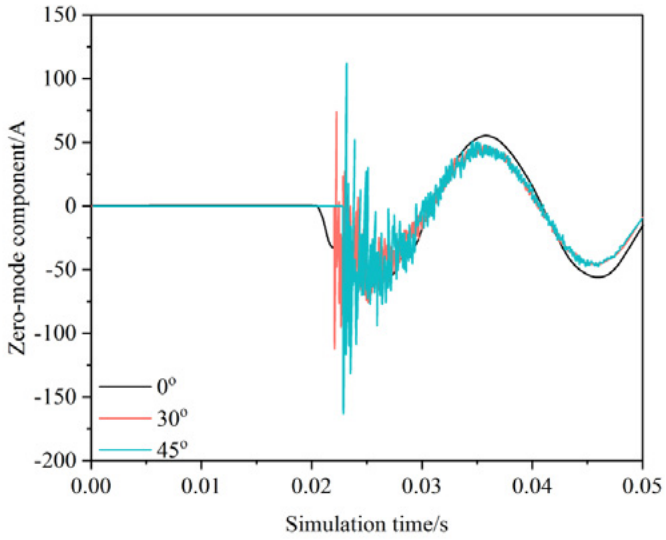

(c) Waveform diagram of zero mode component at point N

Figure 5. Waveform diagram of zero mode component of different faults

https://doi.org/10.17993/3ctecno.2024.v13n1e45.35-55

Different fault location fault initial phase angle of 0 °, 30 °, 45 °, power cable fault point localization simulation results shown in Table 1, in different fault initial phase angle, the algorithm proposed in this paper can accurately determine the fault section, and determine the results of the fault section with the occurrence of faults are consistent with the positioning results of the relative error in the majority of the 1% or less, to meet the demand for three-dimensional simulation of fault point localization accuracy of power cables.

Table 1 Short-circuit fault location results for different initial phase angles

Fault distance /km	Initial fault phase Angle/°	Fault location/km	Ranging error/%
6	0	5.961	0.65
	30	6.047	0.78
	45	5.957	0.72
11	0	11.102	0.93
	30	11.105	0.95
	45	11.096	0.87
34	0	34.021	0.06
	30	34.024	0.07
	45	33.948	0.15
54	0	54.014	0.03
	30	54.021	0.04
	45	53.984	0.03
63	0	63.038	0.06
	30	62.896	0.17
	45	63.026	0.04

3.2. COMPARATIVE ERROR ANALYSIS BETWEEN DIFFERENT ALGORITHMS

Comparing this paper's algorithm with EMD, Wavelet decomposition, SKT algorithm, Table 2 shows the error analysis of four algorithms for fault localization, and the data show that the error of the fault localization method proposed in this paper is lower than that of the other two fault localization errors. In single-phase ground fault, the average error of this paper's algorithm is 0.112km, and the average errors of EMD decomposition, traditional wavelet, and synchronous squeezed SWT decomposition are 0.32km, 0.282km, and 0.241km, respectively. in two-phase grounded short-circuit fault, the average error of this paper's algorithm is 0.126km, the average error of EMD

https://doi.org/10.17993/3ctecno.2024.v13n1e45.35-55

decomposition, traditional wavelet, and synchronous squeezed SWT decomposition are 0.304km, respectively. 0.304km, 0.272km, 0.227km respectively. the proposed method based on wavelet transform and GA-BP power cable fault point 3D simulation localization is better than the traditional wavelet decomposition method, EMD decomposition method, and synchronous squeezing SWT algorithm.

Table 2 Fault location error analysis of the four algorithms

	A Ground connection is faulty	AB Two-phase ground connection fault						
Fault distance /km	EMD	Wavelet decomposition	SKT	Textual algorithm	EMD	Wavelet decomposition	SKT	Textual algorithm
10	486	469	395	250	427	402	337	250
20	415	375	320	199	389	351	297	190
30	424	380	328	192	410	367	314	222
40	351	309	273	109	357	317	271	161
50	318	290	249	126	310	286	222	140
60	290	254	222	96	286	252	216	113
70	240	198	183	44	253	221	195	67
80	294	229	159	78	241	230	150	83
90	205	173	153	17	193	156	140	22
100	173	142	129	4	170	139	128	10

In order to further clarify the advantages and disadvantages of the method proposed in this paper among different algorithms under different fault types, two-phase short circuit and three-phase short circuit fault simulation are set up respectively, and the fault point localization errors are analyzed as shown in Table 3, and the fault localization errors of the method proposed in this paper, which is based on the wavelet transform and the three-dimensional simulation localization of the fault point of GA-BP power cables, are 0.109km and 0.12km, and are smaller than the fault localization errors of EMD decomposition method, traditional wavelet decomposition, and synchronous squeezed SWT algorithm. 0.109km and 0.12km, which are smaller than the fault localization errors of EMD decomposition method, traditional wavelet decomposition, and synchronous squeezing SWT algorithm, so the method proposed in this paper is suitable for fault point localization of power cables with different fault types.

https://doi.org/10.17993/3ctecno.2024.v13n1e45.35-55

Table 3 Fault location error analysis of four algorithms

	AB Two-phase short-circuit fault	ABC Three-phase short circuit fault						
Fault distance /km	EMD	Wavelet decomposition	SKT	Textual algorithm	EMD	Wavelet decomposition	SKT	Textual algorithm
10	455	444	370	238	408	381	320	239
20	396	350	305	190	373	330	285	214
30	405	359	308	180	394	352	298	213
40	336	297	288	124	342	302	260	155
50	293	280	238	122	294	279	213	134
60	284	252	222	102	284	254	217	113
70	222	194	179	46	241	214	183	68
80	223	218	168	56	227	220	148	30
90	194	168	146	21	182	152	138	20
100	168	136	122	8	162	134	123	11

3.3. ERROR ANALYSIS IN A NOISY BACKGROUND

Under two background noise environments, white noise and colored noise, the signal-to-noise ratios are taken as 0dB, -10dB, -15dB, -20dB, and 300 Monte Carlo experiments are carried out for the generalized correlation, quadratic correlation, and this paper's algorithms, respectively, and the statistical results of the simulation of time delay estimation are obtained as shown in Table 4. The results use the time delay estimation mean and root mean square error (is the estimated value and *a* is the actual time delay value, which is 300) as the performance evaluation criteria. The "-" horizontal line indicates that the value is no longer of reference value because the estimation error is too large. Analyzing the data in the table, it can be seen that at not too low signal-to-noise ratios, all three types of algorithms can give accurate estimation results regardless of whether the background noise is white or colored noise. However, in the case of low signal-to-noise ratio, when the white noise signal-to-noise ratio is -20dB, only the error of this algorithm is still within the controllable range, at this time, the mean square error is 0.057, while the white noise signal-to-noise ratio is -15dB, the generalized correlation and the quadratic correlation error is no longer a reference value, at this time, the mean square error of this algorithm is 0.076. The algorithm of this paper has a certain inhibition effect on the noise, and its effect is more desirable than that of the other two methods. The effect is more ideal than the other two methods. Under the same signal-to-noise ratio, for the three delay

https://doi.org/10.17993/3ctecno.2024.v13n1e45.35-55

estimation algorithms, the estimation performance in the case of white Gaussian background noise is significantly better than that in the case of colored Gaussian background noise.

Table 4 Simulation statistical results of delay estimation

SNR		White noise			Colored noise		
		Generalized correlation	Secondary correlation	Textual algorithm	Generalized correlation	Secondary correlation	Textual algorithm
0dB	Mean	300.04	299.96	300.02	299.95	300.05	300.02
	Mean square error	13	11	12	34	49	25
-10dB	Mean	299.89	300.07	299.96	299.87	300.116	300.05
	Mean square error	42	42	22	214	198	53
-15dB	Mean	301.394	298.83	300.28	—	—	299.18
	Mean square error	85	44	34	—	—	76
-20dB	Mean	—	—	298.18	—	—	298.14
	Mean square error	—	—	57	—	—	122

4. CONCLUSION

In this study, a new 3D simulation localization method for power cable fault points is developed by combining wavelet transform and neural network techniques. Experimental results show that the method shows high accuracy and stability in different types of fault localization. Specifically, in the case of single-phase ground fault and two-phase grounded short-circuit fault, the average localization errors of the proposed method are 0.112 km and 0.126 km, respectively, which are much lower than those of the traditional EMD decomposition, traditional wavelet, and synchronous squeezed SWT decomposition methods. In addition, the proposed method shows good adaptability under different fault initial phase angles, and the error is controlled within 1%, which proves its effectiveness under different fault scenarios.

The method also shows excellent performance in noisy environments. Especially in the case of low signal-to-noise ratio, the method proposed in this paper shows better noise immunity and maintains lower localization error compared with traditional methods. This feature makes the method more valuable in practical power system operation and maintenance, especially in complex noise environments.

The proposed three-dimensional simulation localization technique for power cable faults based on wavelet transform and GA-BP neural network not only achieves significant results in improving the localization accuracy, but also significantly

https://doi.org/10.17993/3ctecno.2024.v13n1e45.35-55

improves the ability of anti-noise interference. The development of this technology will bring important practical application value to the fault detection and maintenance of the power system, and help to improve the reliability and stability of the power system.

REFERENCES

(1) Nguyen, T. H., & Lee, D. C. (2017). Protection of the MMCs of HVDC transmission systems against DC short-circuit faults. Journal of Power Electronics.

(2) Lee, S. J., Kang, S. Y., Park, M., Won, D. Y., & Yang, H. S. (2020). Performance analysis of real-scale 23 kV/60 MVA class tri-axial HTS power cable for real-grid application in Korea. Energies, 13(8), 2053.

(3) Chen, Z., Kleijn, R., & Lin, H. X. (2022). Metal requirements for building electrical grid systems of global wind power and utility-scale solar photovoltaic until 2050. Environmental Science & Technology.

(4) Khalil, A. R., Howard, I. M., Forbes, G. L., Sultan, I. A., & McKee, K. K. (2017). Design and installation of subsea cable, pipeline and umbilical crossing interfaces. Engineering Failure Analysis.

(5) Reda, A., Abu-Siada, A., Howard, I. M., & McKee, K. K. (2018). A testing platform for subsea power cable deployment. Engineering Failure Analysis, 96, 142-157.

(6) Ulku, I., & Alabas-Uslu, C. (2020). Optimization of cable layout designs for large offshore wind farms. International Journal of Energy Research, 44(8).

(7) Kwon, G.-Y., Lee, C.-K., Shin, & Yong-June. (2019). Diagnosis of shielded cable faults via regression-based reflectometry. IEEE Transactions on Industrial Electronics.

(8) Brothers, S. (2018). Finding fault with cabling connections. Electrical Engineering (OCT.), 8-8.

(9) Suyang, Wang, Jianmei, Chuang, Zhang, & Yang, et al. (2019). Synchronous online diagnosis of multiple cable intermittent faults based on chaotic spread spectrum sequence. IEEE Transactions on Industrial Electronics, 66(4).

(10) Torwelle, P., Bertinato, A., Raison, B., Le, T. D., & Petit, M. (2022). Fault current calculation in MTDC grids considering MMC blocking. Electric Power Systems Research (Jun.), 207.

(11) Li, G., Chen, J., Li, H., Hu, L., Zhou, W., & Zhou, C., et al. (2022). Diagnosis and location of power cable faults based on characteristic frequencies of impedance spectroscopy. Energies, 15.

(12) Li, M., Bu, J., Song, Y., Pu, Z., & Xie, C. (2021). A novel fault location method for power cables based on an unsupervised learning algorithm. Energies, 14(4), 1164.

(13) Sommervogel, L. (2020). Various models for faults in transmission lines and their detection using time domain reflectometry. Progress in Electromagnetics Research C, 103, 123-135.

(14) Tian, Y., Zhao, Q., Zhang, Z., Li, L., & Crossley, P. (2018). Current-phase-comparison-based pilot protection for normally closed-loop distribution network with underground cable. International Transactions on Electrical Energy Systems, 28(9), e2733.1-e2733.19.

(15) Li, Z., Yang, H., Yang, F., Tan, T., Lu, X., & Tian, J. (2022). An infrared image based state evaluation method for cable incipient faults. Electric Power Systems Research.

https://doi.org/10.17993/3ctecno.2024.v13n1e45.35-55

(16) Siodla, K., Rakowska, A., & Noske, S. (2021). The proposal of a new tool for condition assessment of medium voltage power cable lines. Energies, 14.

(17) Samet, H., Tajdinian, M., Khaleghian, S., & Ghanbari, T. (2021). A statistical-based criterion for incipient fault detection in underground power cables established on voltage waveform characteristics. Electric Power Systems Research, 197, 107303.

(18) Li, C., Chen, J., Zhang, W., Hu, L., Cao, J., & Liu, J., et al. (2021). Influence of arc size on the ignition and flame propagation of cable fire. Energies, 14.

(19) Lacerda, V. A., Monaro, R. M., & Coury, D. V. (2021). Fault distance estimation in multiterminal HVDC systems using the Lomb-Scargle periodogram. Electric Power Systems Research, 196, 107251.

https://doi.org/10.17993/3ctecno.2024.v13n1e45.35-55